Changes in French weather pattern seasonal frequencies projected by a CMIP5 ensemble

Pierre Brigode, M. Gérardin, P. Bernardara, J. Gailhard, P. Ribstein

Changes in French weather pattern seasonal frequencies projected by a CMIP5 ensemble

Brigode P.[1,2,*], Gérardin, M.[2], Bernardara P.[1], Gailhard J.[3] and Ribstein P.[2]

[1] LNHE, R&D, Electricité de France (EDF), Chatou, France.

[2] UMR 7619 Metis, Sorbonne Université, Paris, France.

[3] DTG, DMM, Electricité de France (EDF), Grenoble, France.

[*] *Now in: Université Côte d'Azur, CNRS, OCA, IRD, Géoazur.*

Corresponding author: Pierre Brigode (pierre.brigode@unice.fr)

Keywords:

Weather pattern frequency; future weather pattern frequency; CMIP5; French climatology.

Abstract (up to 300 words):

Over the last decades, General Circulation Model (GCM) simulations have been regularly evaluated in terms of their ability to reproduce the historical frequency of significantly recurrent Weather Patterns (WP) observed at the regional scale. Thus, a good simulation of the frequency of these particular WP by the GCM is generally conditioning the good representation of the regional statistics of surface variables such as temperature and precipitation. In this paper, the seasonal frequency of eight particular WP have been calculated using the daily geopotential height fields simulated by an ensemble of 26 CMIP5 GCM. These WP are known as significantly influencing the French regional hydro-climatology in terms of both frequency of low flows and high precipitation events. Four different bias correction methods have been applied on the simulated geopotential height fields before the calculation of the seasonal WP frequencies. The GCM ensemble showed overall good performances in terms of the simulation of WP seasonal frequencies. The application of a spatially and temporally nonhomogenous correction of simulated geopotential height fields improved significantly the simulation of WP frequencies for the four seasons. Finally, the evolution of the WP frequencies over the next century has been quantified. Three WP (WP2, WP4 and WP8) have pronounced seasonal changes, with WP2 and WP4 being less frequent in summer and autumn seasons, respectively, while WP8 being more frequent over spring, summer and autumn seasons. The strong simulated frequency evolution of WP2 and WP8 is an interesting result, which predicts the climate to be drier with time for France. Thus, WP2 (western oceanic circulation), grouping rainy days over the northern France region, is simulated as less frequent in future summers, while WP8 (Anticyclonic situations), which groups non-rainy days over France, is simulated as more frequent in future summers.

1 INTRODUCTION

Since several decades, meteorologists and climatologists have worked on the identification of particular atmospheric circulations patterns that are recurrently observed at the regional scale and that are strongly affecting the spatial and the temporal variability of surface variables, such as temperature and precipitation (e.g. over Europe by Plaut & Simonnet, 2001 ; Cassou *et al.*, 2005 ; Boé & Terray 2008). Different classification methods are used for identifying a limited number of significantly recurrent circulation patterns (see Huth *et al.,* 2008 for a review), generally based on the analysis of atmospheric circulation variables such as Sea Level Pressure (SLP) or geopotential heights (Vautard, 1990; Michelangeli *et al.*, 1995). In the literature, the obtained recurrent circulations patterns have different names and are usually referenced as (weather, atmospheric, climate or circulation) regimes, types or patterns, based on their properties (Stephenson *et al.*, 2004). Philipp *et al.* (2007) opposed the weather regimes (WR) to the weather patterns (WP) in terms of their spatial and temporal characteristics. The WR are usually one to four "quasi-stationary states of the large-scale circulation system" defined at the 10-day timescale, while the WP are more numerous situations defined at a finer spatial scale since being devoted to the classification of the circulation system on a daily timescale. The utility of WP classifications for quantifying the influence of large-scale climate drivers on hydro-climatological variability has been discussed by several studies, mainly arguing that WP are defined at an intermediate spatial scale between WR and local climatic observations (e.g. Giuntoli *et al.*, 2013 ; Brigode *et al.*, 2013a, 2013b).

Recently, WP frequencies have thus been used as a conditioning variable for the statistical modelling of extreme hydro-climatological values (e.g. Planchon *et al.* 2009; Brigode *et al.*, 2013b). For example, several studies successfully linked WP (or circulation-related variables) to flood statistics at the regional scale (e.g. Nied *et al.*, 2014; Wilby & Quinn, 2013; Renard & Lall, 2014). In the framework of the statistical modelling of extreme precipitation, Garavaglia *et al.* (2010, 2011) proposed an eight WP classification for sub-sampling precipitation events over France in terms of their synoptic origin. Tramblay *et al.* (2011, 2013) used the same WP classification as conditioning variables in a non-stationary extreme value frequency analysis and showed the soundness of using this framework for the statistical modelling of extreme precipitation in southern French regions. Furthermore, Giuntoli *et al.* (2013) found significant correlations between these WP and low flows over France, highlighting again the strong link between these WP and the seasonal French hydro-climatology.

These significant links are of particular interest in the context of the quantification of regional climate change impacts. Under the (strong) hypothesis that the statistical relationships observed over the historical period hold unchanged under climate changes, WP classifications can be used to downscale and transform changes of atmospheric circulations into changes of regional surface variables (Boé & Terray, 2008). Nevertheless, this approach is based on the other hypothesis that atmospheric circulations are better simulated by the Global Circulation Models (GCM) than surface variables such as precipitation. At the global scale, numerous studies showed that large-scale features of the atmospheric circulation are among the variables that GCM represent with the best robustness (e.g. Covey *et al.*, 2003; Räisänen, 2007), even though the ability of GCM to simulate changes in atmospheric circulation is recently questioned (e.g. Palmer, 1999; Corti *et al.*, 1999; Hsu & Zwiers, 2001; Gillett *et al.*, 2003; Shepherd, 2014; Hall, 2014; Murawski *et al.*, 2016).

79   WR and WP classifications have been widely used as a way to evaluate GCM outputs in terms of
80   their ability to reproduce WR and WP frequencies over a target region (Sheridan & Lee, 2010).
81   Frequencies of simulated WP have been evaluated over different regions, such as the Euro-Atlantic
82   region (e.g. Demuzere *et al.*, 2009; Handorf & Dethloff, 2012 and Pastor & Casado, 2012), the Arctic
83   region (e.g. Cassano *et al.*, 2006), the northwestern Iberian Peninsula (e.g. Lorenzo *et al.*, 2011) and
84   the Northwest America region (e.g. McKendry *et al.*, 2006). Anagnostopoulou *et al.* (2008) used the
85   500 hPa geopotential height (Z_{500}) and the 1000-500 hPa thickness fields for WP classification over the
86   eastern Mediterranean region and revealed several differences between observed WP frequencies
87   and the frequencies simulated by the considered GCM (HadAM3P), with, for example, an
88   overestimation of the summer frequency of anticyclonic situations. Sanchez-Gomez *et al.* (2009)
89   evaluated the performances of an ensemble of 13 Regional Climate Models (RCM) forced by a
90   reanalysis (ERA40) in terms of the simulation of WR over the Euro-Atlantic region and highlighted the
91   good performances of the ensemble in terms of the simulation of the mean WR frequency. During the
92   last years, the GCM outputs of the fifth Coupled Model Intercomparison Project (CMIP5, Taylor *et al.*
93   (2012)) have been evaluated with the same methodology over different regions (e.g. by Belleflamme
94   *et al.* (2013) over Greenland and by Dunn-Sigouin & Son (2013); Hertig & Jacobeit (2014) and Ullmann
95   *et al.* (2014) over the Northern hemisphere), and the CMIP5 GCM appear to represent generally well
96   the observed WR. Nevertheless, Belleflamme *et al.* (2014) and Santos *et al.* (2016) illustrated the
97   limitations of two different GCM ensembles in simulating seasonal WP frequency over Europe for the
98   recent decades. The ability of GCM to simulate WR and WP frequency seem thus to depend on the
99   GCM considered, on the spatial scale considered and on the WR and WP classification method used.

100   The general aim of the paper is to quantify the frequency changes of the eight French WP previously
101   defined by Garavaglia *et al.* (2010) simulated by an ensemble of 26 CMIP5 GCM over the 21st century.
102   Before studying future WP frequency changes, the performances of the GCM ensemble will be
103   quantified over the historical period (here 1979-2004), using four different bias correction method
104   applied on the GCM geopotential heights fields.

105

2   DATASETS

2.1   Reanalysis of geopotential height fields

The ERA-Interim global atmospheric reanalysis (Dee *et al.*, 2011, noted ERAi hereafter) has been used as reference for geopotential height fields for the historical period. This gridded dataset is available from 1979, at a 0.75° spatial resolution and at a 12-hour temporal resolution. Two levels have been considered in this study, namely (i) the geopotential height field at 1000 hPa (noted Z_{1000} hereafter) and (ii) the geopotential height field at 700 hPa (noted Z_{700} hereafter), both at 0h for each day. The historical period considered in this study is 1979-2004.

2.2   GCM geopotential height field outputs

Daily Z_{1000} and Z_{700} outputs from 26 GCM have been considered in this study. All outputs have been generated within the fifth phase of the Coupled Model Intercomparison Project (CMIP5, Taylor *et al.*, 2012). The GCM studied are listed in table S1. The daily outputs of three different experiments have been used:

- The "historical" experiment, which consists of a simulation of the recent past (1950-2005 period) under the historical forcing;

- The "RCP4.5" experiment, which extends the "historical" experiment by simulating the future (2006-2100) under the RCP4.5 emission scenario (radiative forcing surplus of 4.5 W.m^{-2} in 2100).

- The "RCP8.5" experiment, which extends the "historical" experiment by simulating the future (2006-2100) under the RCP8.5 emission scenario (radiative forcing surplus of 8.5 W.m^{-2} in 2100).

The two emission scenarios considered here are members of the four Representative Concentration Pathway (RCP) scenarios considered in the CMIP5 experiments (Moss *et al.*, 2010).

Only the first member (named r1ip1) from the historical, RCP4.5 and RCP8.5 experiments have been considered for each GCM. The simulated Z_{1000} and Z_{700} fields have been spatially interpolated on the ERAi grid (0.75° grid spacing). The historical experiment outputs are considered over the 1979-2004 period (period of availability of the ERAi dataset) and the future experiment outputs are considered over the 2006-2098 period.

Several GCM outputs being produced by climate models with structural similarities (e.g. the bcc-csm1-1 outputs and the bcc-csm1-1-m outputs), a sub-sample of the 26 outputs has also been considered. Thus, the seasonal WP frequencies simulated using outputs produced by similar climate models (i.e. developed by the same institution) were averaged. The Table S1 presents the merging considered for the constitution of the second GCM ensemble (noted INS ensemble hereafter, where INS stands for "institution"), composed by 15 GCM outputs out of the 26 available.

2.3   Precipitation reanalysis

As an illustration of the regional precipitation patterns associated to each WP, the E-OBS daily precipitation reanalysis (Haylock *et al.*, 2008, version 16.0) is used in this study. This reanalysis provides daily precipitation amounts at a 0.25° resolution. This dataset has been used over Western Europe and the 1979-2004 period.

143   3   METHODOLOGY

144   This section aims at describing the WP classification considered, the bias correction methods used and
145   the frequency analysis methodology, all performed in the R-project environment (R Core Team, 2016,
146   http://www.r-project.org/).

147   3.1   The WP classification method

148   *3.1.1   Average synoptic situation of the eight French WP*

149   The WP considered in the paper are the eight French WP defined by Garavaglia *et al.* (2010). These
150   WPs have been defined at the daily time step through a classification of "rainy days" over southern
151   France for the 1956-1996 period (see Garavaglia *et al.*, 2010 and Brigode *et al.*, 2013b for more details
152   on the rainy days classification method). For example, the first WP (WP1) is constituted by 668 rainy
153   days of the 1956-1996 period.

154   The synoptic characteristics of each of the eight WP have then been calculated by averaging the
155   synoptic situations of the different days constituting each WP. Thus, the WP1 synoptic situation is the
156   average of the synoptic situations of the 668 rainy days previously identified as constituting the WP1.
157   Four geopotential height fields are considered for the synoptic description of each day and thus of
158   each WP:

159   1.   the Z_{1000} field at 0h,

160   2.   the Z_{1000} field at 24h,

161   3.   the Z_{700} field at 0h,

162   4.   the Z_{700} field at 24h.

163   In this study, the average synoptic situation of each WP has been estimated with the ERAi geopotential
164   reanalysis (available from 1979, see section 2) and thus computed over the 1979-1996 period.
165   Geopotential height fields have been considered over 504 ERAi grid points, centered over southern
166   France (-7.50° to 12.75° of longitude and 37.50° to 50.25° of latitude). Figure 1 shows the average Z_{700}
167   field at 24h of each WP, estimated over the 1979-1996 period, and the spatial coverage of the 504
168   ERAi grid points.

169   *3.1.2   Classification of the historical period*

170   In order to obtain a daily classification for the studied historical period, each past day is assigned to
171   one of the eight WP by computing distances between the synoptic situation of the studied day and
172   each WP. Teweles & Wobus (1954) distances (noted D_{TW} hereafter) are calculated to find the closest
173   WP to each considered day (see Brigode *et al.*, 2013a, 2013b for more details). D_{TW} focuses on air flows
174   since this distance involves gradients of absolute values of geopotential heights (Woodcock, 1980;
175   Obled *et al.*, 2002; Bontron, 2004; Wetterhall *et al.*, 2005, Brigode *et al.*, 2016). The formula for
176   estimating D_{TW} between two synoptic situations (Z1) and (Z2) characterized by geopotential height
177   fields on a gridded domain oriented south-north (index *i*) and west-east (index *j*) is :

178
$$D_{TW} = \frac{\sum_{i,j}\left|e_G^i\right| + \sum_{i,j}\left|e_G^j\right|}{\sum_{i,j}\left|G_L^i\right| + \sum_{i,j}\left|G_L^j\right|} \times 100$$

179   where e_G is the difference, around a given grid point, between the Z1 and Z2 geopotential gradients,
180   while G_L is the maximum of these two gradients in the direction considered (*i* or *j*):

$$\left|e_G^i\right| = \left|(Z1_{i,j} - Z1_{i+1,1}) - (Z2_{i,j} - Z2_{i+1,1})\right|$$

$$\left|e_G^j\right| = \left|(Z1_{i,j} - Z1_{i,j+1}) - (Z2_{i,j} - Z2_{i,j+1})\right|$$

$$\left|G_L^i\right| = \max\left(\left|Z1_{i,j} - Z1_{i+1,1}\right|, \left|Z2_{i,j} - Z2_{i+1,1}\right|\right)$$

$$\left|G_L^j\right| = \max\left(\left|Z1_{i,j} - Z1_{i,j+1}\right|, \left|Z2_{i,j} - Z2_{i,j+1}\right|\right)$$

185   D_{TW} ranges from 0 for two identical geopotential fields and 200 for two opposite geopotential fields.
186   The final score between one day and one WP is the sum of four D_{TW} distances: (i) the D_{TW} between the
187   Z_{700} fields at 0h, (ii) the D_{TW} between the Z_{1000} fields at 24h, (iii) the D_{TW} between the Z_{700} fields at 0h
188   and (iv) the D_{TW} between the Z_{700} fields at 24h. The D_{TW} calculation is illustrated in figure 1, which shows
189   the eight D_{TW} calculated between one particular day (21th September 1992) and the average synoptic
190   situation of the eight French WPs for the Z_{700} fields at 24h. The minimal D_{TW} is found for the WP4
191   (D_{TW}=48.4). The three other calculations of D_{TW} for that particular day (Z_{1000} at 0h, Z_{1000} at 24h and Z_{700}
192   at 0h) are summarized in the table 1. The sum of the four D_{TW} is minimal for the WP4 (D_{TW}=205.5): the
193   21th September 1992 is thus attributed to the WP4. Note that this synoptic situation has generated a
194   considerable amount of precipitation in South-Eastern France, with more than 300 mm of precipitation
195   observed locally that day (Benech *et al.*, 1993), generating a catastrophic and deadly flash flood of the
196   Ouvèze river (Sénési *et al.*, 1996).

197

198   **Table 1:** D_{TW} distances calculated between the 21th September 1992 synoptic situation and the average
199   synoptic situation of the eight French WPs for the Z_{1000} and Z_{700} fields at 0h and at 24h. In this case, the
200   21th September 1992 is finally attributed to the WP4.

	WP1	WP2	WP3	**WP4**	WP5	WP6	WP7	WP8
Z_{1000} at 0h	91.9	101.1	85.3	**67.9**	95.2	81.1	70.7	96.8
Z_{1000} at 24h	92.0	91.7	67.6	**52.2**	89.6	84.1	64.2	99.6
Z_{700} at 0h	62.5	73.3	49.7	**36.9**	63.4	63.6	46.1	70.4
Z_{700} at 24h	74.7	82.1	59.0	**48.4**	79.8	71.4	56.8	86.6
D_{TW} sums	321.1	348.2	261.6	**205.5**	328.1	300.3	237.7	353.4

201
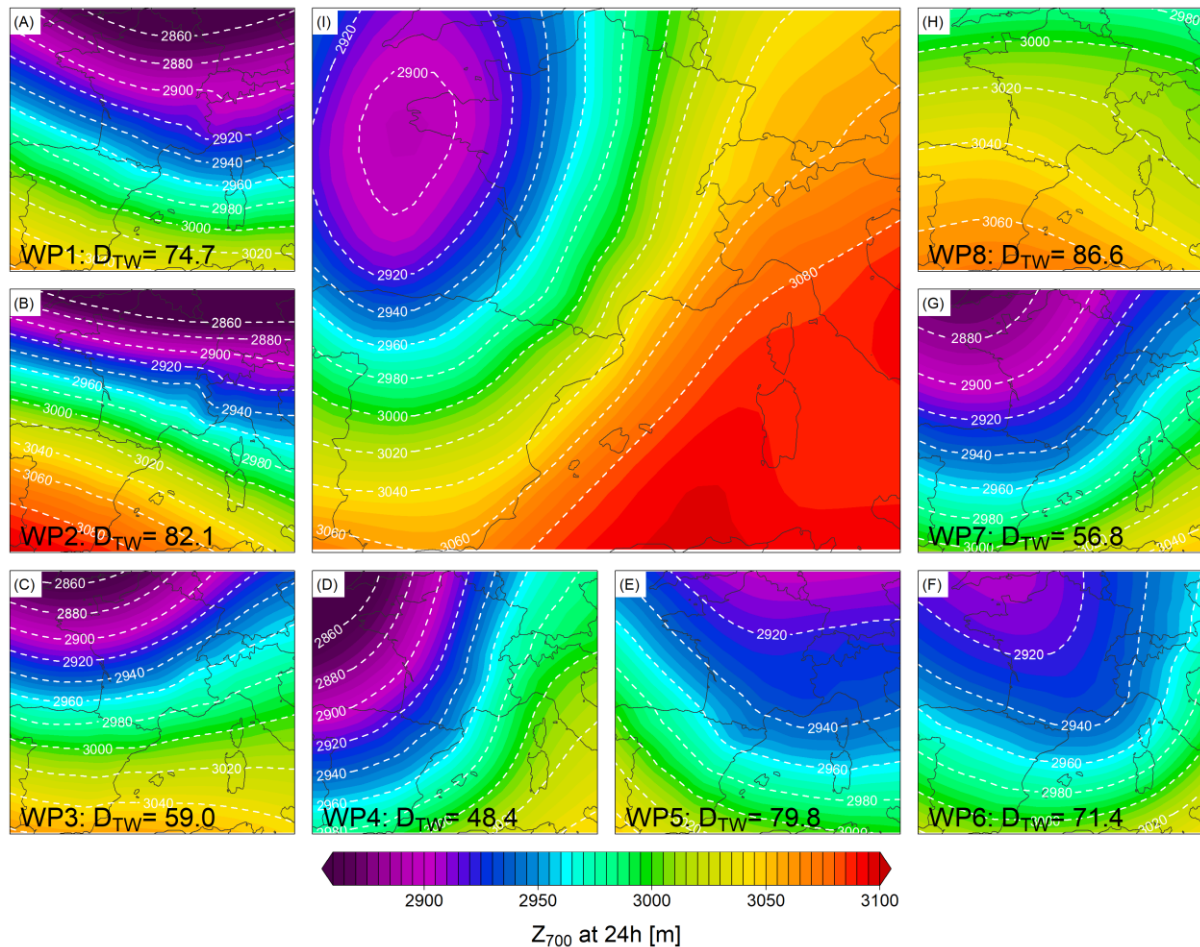
Figure 1: *Comparison between the Z_{700} synoptic situation of the 21th September 1992 (at 24h, panel I) and the Z_{700} situation of the eight French WP (panels A to H). The D_{TW} distances calculated between these geopotential fields are given on each panel.*

### 3.1.3   Meteorological description of the eight French WP

The eight French WPs are described in the figures 2.1 and 2.2, in terms of average ERAi Z_{700} and Z_{1000} fields at 0h, E-OBS regional precipitation pattern and seasonal frequencies, calculated over the 1979-2004 period. The eight WP can be grouped in terms of their general atmospheric flow direction (cf. column (a) of the figures 2.1 and 2.2, showing average SLP for each WP):

- WP1 (Atlantic Wave), WP2 (Steady Oceanic) and WP3 (Southwest Circulation) correspond to westerly oceanic circulation, grouping days particularly rainy over the Alps, the Northwestern part of France and the Western part of France, respectively. The WP2 is one of the most frequent over the year, especially during the winter season.

- WP4 (South Circulation), WP6 (East Return) and WP7 (Central Depression) correspond to Mediterranean circulations, grouping days particularly rainy over the Southeastern part of France. WP6 and WP7 days are relatively rarely observed.

- The WP5 (Northeast Circulation) corresponds to continental circulations, grouping days not particularly rainy over France.

221   • Finally, the WP8 (Anticyclonic) corresponds to high pressure situations and thus groups non-
222   rainy days. This French WP is the most frequent, especially in summer.

223
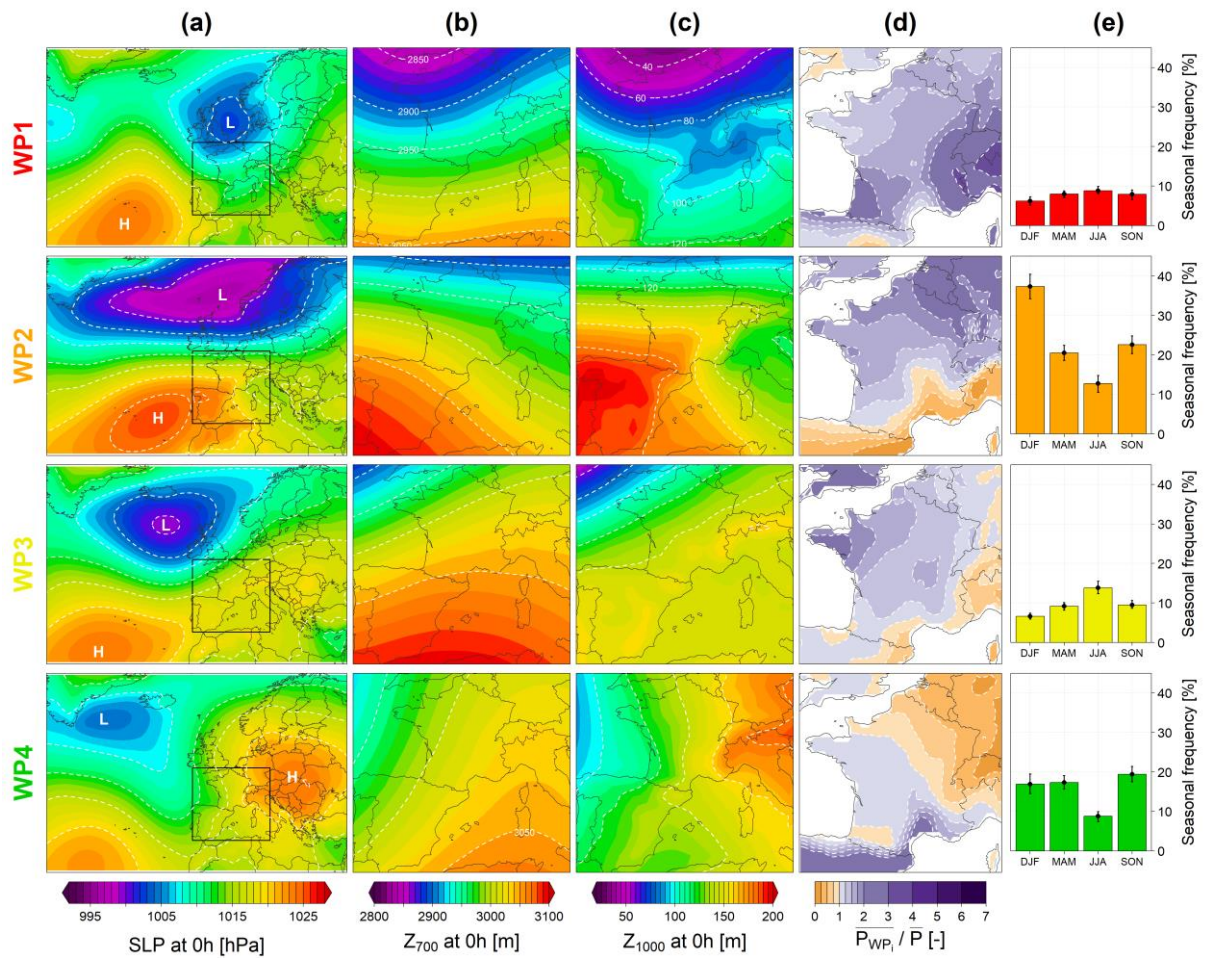
224

225   *Figure 2.1:* *Description of the WP1 to WP4: (a) average ERAi SLP at 0h, (b) average ERAi Z_{700} at 0h, (c)*
226   *average ERAi Z_{1000} at 0h, (d) ratio between the E-OBS mean precipitation amounts and the general*
227   *precipitation amount (considering all WP) and (e) seasonal frequency of the WP, estimated over the*
228   *1979-2004 period.*

229
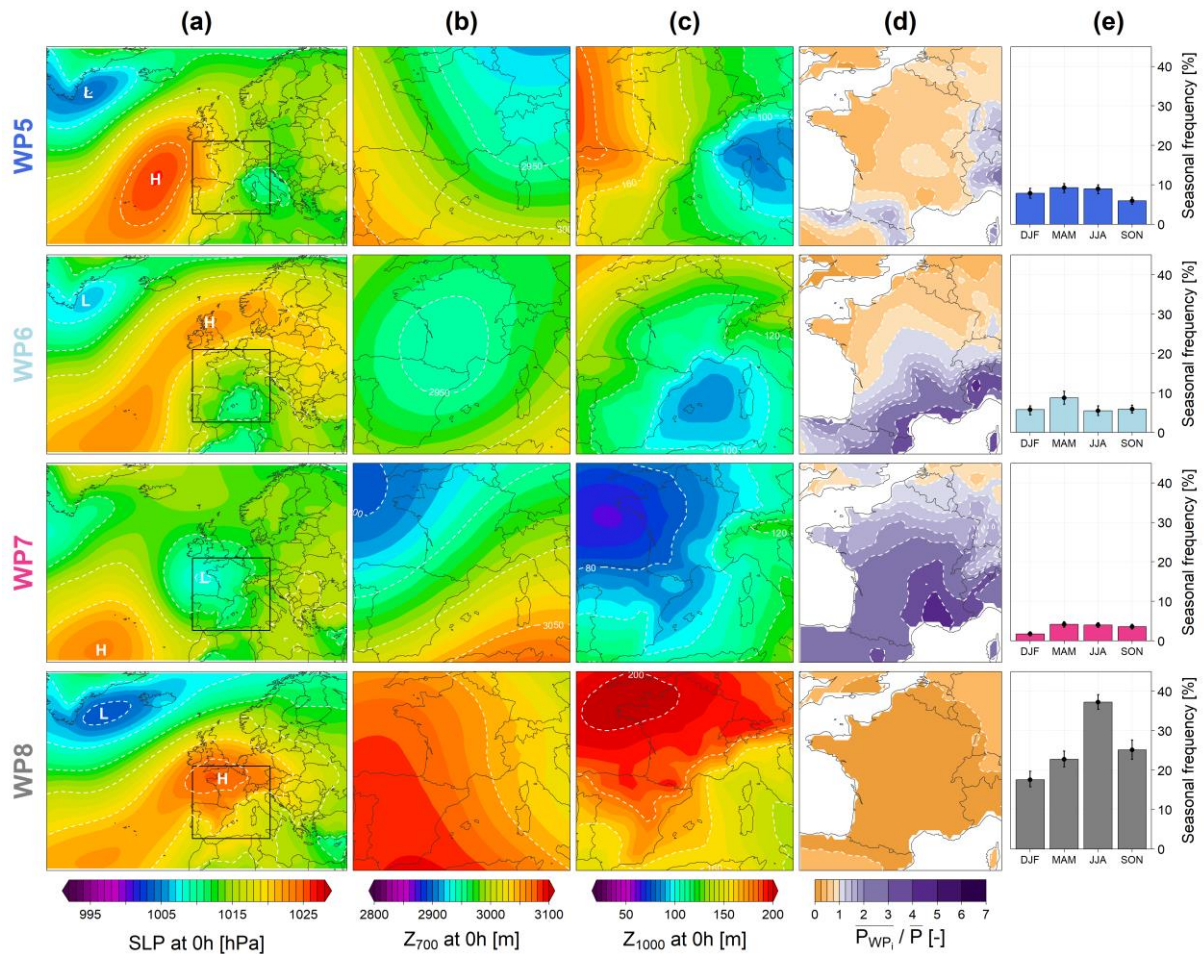
Figure 2.2: Description of the WP5 to WP8: (a) average ERAi SLP at 0h, (b) average ERAi Z_{700} at 0h, (c) average ERAi Z_{1000} at 0h, (d) ratio between the E-OBS mean precipitation amounts and the general precipitation amount (considering all WP) and (e) seasonal frequency of the WP, estimated over the 1979-2004 period.

3.2   Classification of the daily GCM outputs

The classification of the geopotential height fields simulated by the GCM has been done with the same methodology, i.e. by calculating D_{TW} between each simulated day (characterized by four synoptic situations: Z_{1000} at 0h, Z_{1000} at 24h, Z_{700} at 0h and Z_{700} at 24h) and the ERAi average situations of the eight French WP (also being characterized by four synoptic situations). The sum of the four D_{TW} is calculated for each simulated day and each WP, and the WP with the minimal D_{TW} sum is attributed to the studied day.

3.3   Geopotential height bias correction methods

While most of the studies on the GCM WP simulation used uncorrected GCM outputs, it is noteworthy that Demuzere *et al.* (2009) and Lorenzo *et al.* (2011) found better performances of GCM in terms of frequencies if the SLP fields used for the classification were bias-corrected before the classification procedure. Thus, the need for bias correction of GCM geopotential height fields before performing WP classification will be tested in this paper, by considering different bias correction methods.

249   D_{TW} distance values have been firstly computed without correcting the GCM geopotential height
250   fields. The WP frequencies obtained by using these uncorrected GCM outputs are named D0 hereafter.
251   Then, four different bias correction methods have been applied to the GCM outputs:

252   1. A spatially homogeneous correction of the geopotential height average values and standard
253   deviations. The outputs of this bias correction method are named D1 hereafter. Note that since
254   D_{TW} are estimated by considering synoptic circulation gradients, a spatially homogeneous
255   correction of average values only is useless: lowering or rising the mean geopotential height
256   fields has no effect on the D_{TW} values.
257   2. A spatially nonhomogeneous correction of the average values. The outputs of this bias
258   correction method are named D2 hereafter.
259   3. A spatially nonhomogeneous correction of the geopotential height average values and standard
260   deviations. The outputs of this bias correction method are named D3 hereafter.
261   4. A spatially nonhomogeneous correction of the monthly average values and standard deviations.
262   The outputs of this bias correction method are named D4 hereafter.

263   To summarize, each GCM output is considered five times: firstly without any bias correction method
264   (outputs named D0) and then after application of the D1, D2, D3 and D4 bias correction methods.

3.4   Seasonal WP frequencies and frequency variability

266   Seasonal frequencies of the eight French WP have been estimated over the 25-year historical period
267   (01/03/1979-29/02/2004) and over 68 25-year periods extracted from the future RCP simulations
268   (2006-2031, 2007-2032, …, 2073-2098). Four 3-month seasons have been defined: the autumn season
269   (September, October and November, noted SON hereafter), the winter season (December, January
270   and February, noted DJF hereafter) the spring season (March, April and May, noted MAM hereafter)
271   and the summer season (June, July and August, noted JJA hereafter). For each season and each WP,
272   frequencies are defined as the percentage of days belonging to the considered WP. The reference
273   observed seasonal frequencies of the eight WP are the seasonal frequencies represented in column (e)
274   of figures 2.1 and 2.2.

275   In order to quantify the WP frequency variability within a time period, a non-parametric bootstrap
276   resampling has been performed. Thus, for each 25-year time period considered, 100 samples of 15
277   randomly chosen years are constructed. Note that no replacements are allowed within this bootstrap
278   resampling, and thus one particular year cannot be resampled twice. These 100 samples are then used
279   to quantify the variability of the frequency by measuring the 90% confidence interval. The dispersion
280   of observed WP frequencies are shown in figures 2.1 and 2.2 for the 1979-2004 period. The observed
281   variability of the seasonal frequencies is limited, the highest variability is observed for the WP2, WP4
282   and WP8. For example, the summer frequency of WP8 ranges between 33.2% and 38.8%.

283

284   # 4   RESULTS

285   ## 4.1   GCM simulations of WP average Z_{1000} and Z_{700}

286   The GCM ensemble outputs have been firstly evaluated in terms of the simulation of the average
287   Z_{700} and Z_{1000} fields for the eight WP, over the 1979-2004 period. Figure 3 summarizes the spatial
288   variability of the Z_{1000} and Z_{700} bias, calculated for each WP as the difference between the GCM
289   ensemble mean fields and the average ERAi fields (presented in the figures 2.1 and 2.2). For Z_{700}, the
290   GCM ensemble appears to overestimate the geopotential heights for the eight WP. The spatial
291   distributions of theses biases reveal a slighter bias over northwestern France (Atlantic Sea). The spatial
292   distribution of Z_{1000} bias changes with WP. For WP1, WP5 and WP7, the GCM ensemble tends to
293   underestimate the Z_{1000} values over northwestern France and to overestimate the Z_{1000} values over the
294   southeastern part of the studied region. For the WP6, the Z_{1000} values are slightly underestimated over
295   the entire studied region. For the other WP (WP2, WP3, WP4 and WP6), the GCM ensemble tends
296   generally to overestimate the Z_{1000} values over the studied region. The spatial variability of biases
297   justified the use of bias correction method that are spatially (D2 to D4) nonhomogeneous.

298
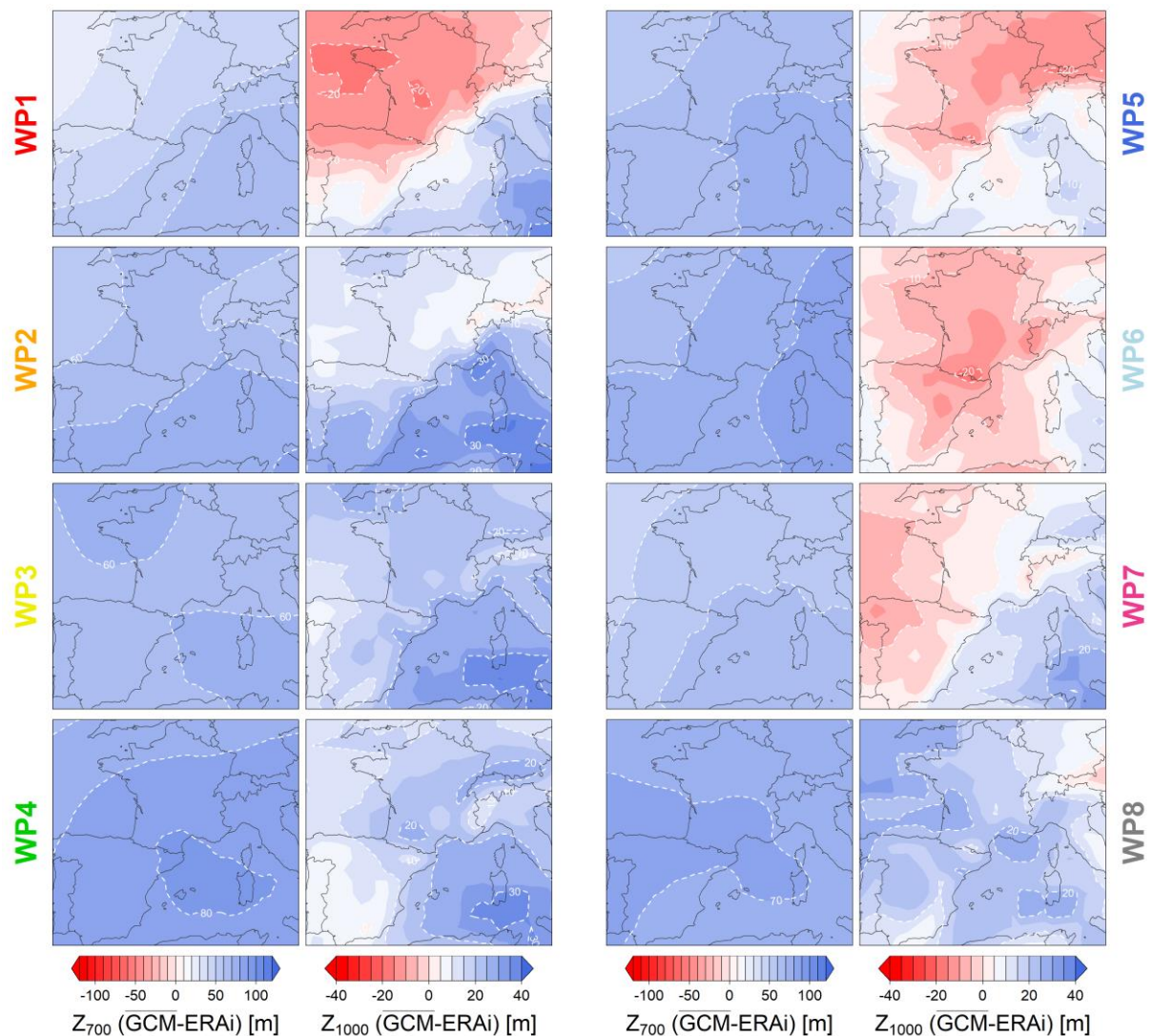
Figure 3: Z_{700} and Z_{1000} geopotential bias calculated for each WP as the difference between GCM ensemble mean and ERAi geopotential height fields.

4.2   Historical seasonal WP frequencies simulated by the GCM ensemble

The GCM ensemble has then been evaluated in terms of simulating historical WP frequencies for the four different seasons considered. Figure 4 presents the observed (ERAi) seasonal WP frequencies estimated over the 1979-2004 period and the WP frequencies simulated by the GCM ensemble (uncorrected and corrected). The seasonal variability of the WP frequencies are generally well simulated by the uncorrected GCM (expect for the WP4). Nevertheless, the frequencies of the two most frequent WP (WP2 and WP8) are poorly simulated, with WP2 frequencies being strongly overestimated and WP8 strongly underestimated. Moreover, the dispersion of the GCM ensemble is large for these two WP as well as for the WP4. The impact of the different bias correction methods on the historical WP frequencies is not straightforward and needs further investigations.

313
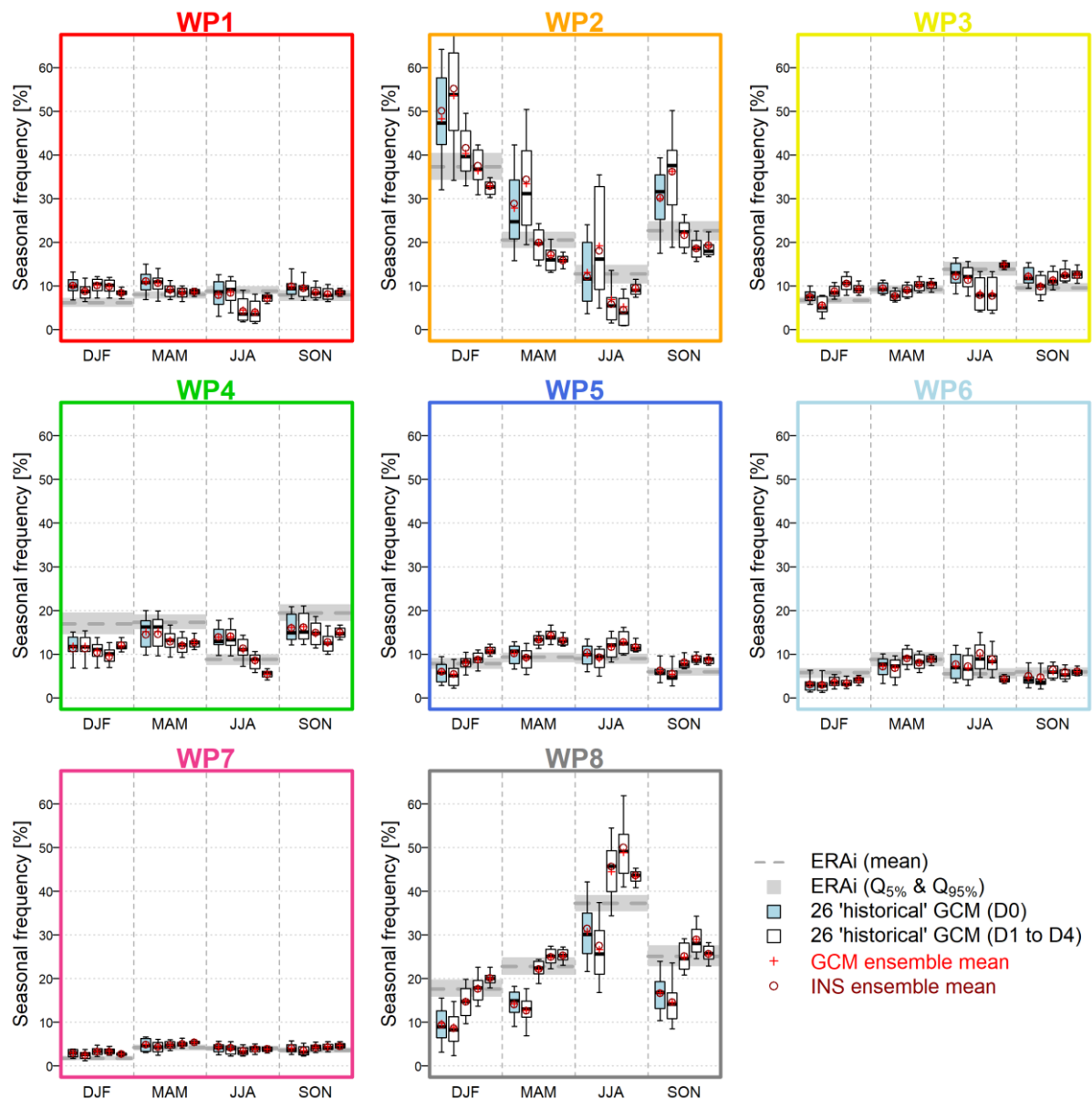
Figure 4: *Seasonal WP frequencies estimated over the 1979-2004 period. The grey rectangles present*
the observed (ERAi) WP frequencies. The boxplots are constructed with the WP frequencies simulated
by the GCM ensembles (GCM and INS) without bias correction (blue boxplots) and with bias corrections
(white boxplots, D1 to D4).

Figure 5 presents the distribution of Euclidean distances calculated, for each season and each bias
correction method, between the vector of the 8 observed WP frequencies and the 26 vectors of 8
simulated WP frequencies. When no bias correction is applied (D0 method), the GCM ensemble is
slightly less performant for DJF season (average distance around 19%) than for other seasons (average
distance around 15.5%). The application of the D1 bias correction method (spatially homogeneous
correction of the geopotential height standard deviations) appears to degrade the performance of the
GCM ensemble in terms of seasonal WP frequencies. Nevertheless, the application of the D2 to D4
correction methods (all spatially inhomogeneous correction methods) improves the GCM ensemble
performances for the DJF, MAM and SON seasons. For the JJA season, only the D4 bias correction

328   method improves the performance of the WP frequency simulation. Overall, the D4 bias correction
329   method (only method implying a spatial and temporal nonhomogenous correction) has the best
330   performances in terms of simulation of the ERAi WP frequencies on the historical period.

331
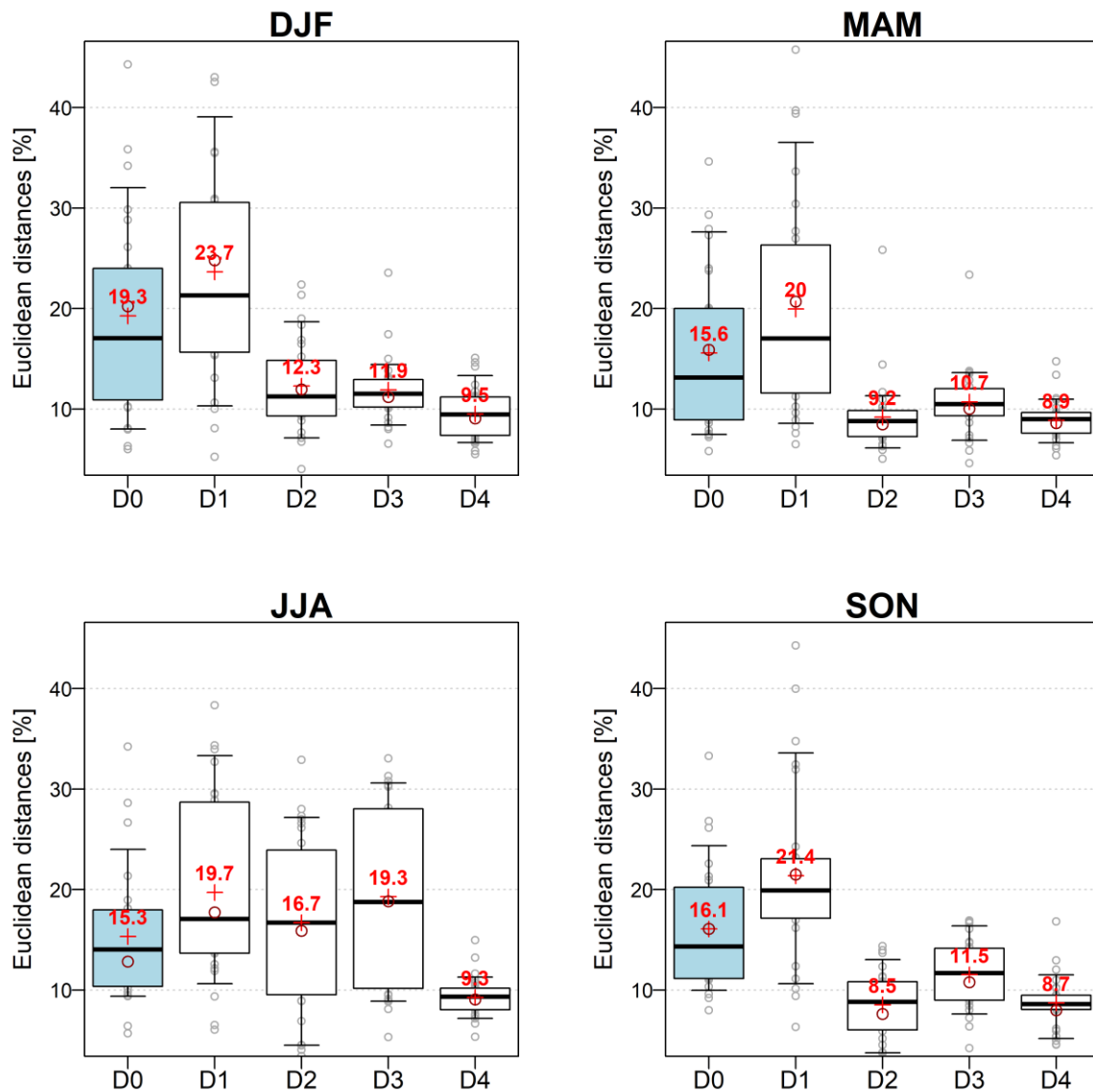
332

333   **Figure 5:** *Distributions of seasonal Euclidean distances calculated, for each season and each bias*
334   *correction method, between the vector of 8 observed WP frequencies and the 26 vectors of 8 simulated*
335   *(GCM) WP frequencies over the 1979-2004 period. The blue boxplots are WP frequencies obtained*
336   *without bias correction, and the white ones are obtained when the bias correction D1 to D4 are applied.*
337   *Red values are mean values of Euclidean distances between WP frequency vectors and grey points are*
338   *individual GCM distances.*

339

4.3   Future evolutions of seasonal WP frequencies

In this section, the changes of WP frequencies simulated by the GCM ensemble are calculated. Regarding the performances obtained by the four different bias correction methods tested (see Section 4.2), only the best method (D4) has been considered for the estimation of future WP frequencies. Thus, future frequencies are calculated with both uncorrected GCM outputs (D0) and GCM outputs corrected with the D4 method.

Figure 6 presents the mean seasonal frequency evolutions simulated by the GCM ensemble, considering both RCP4.5 and RCP8.5 emission scenarios and both GCM outputs without bias correction and GCM outputs corrected with the D4 method. None particular temporal evolutions throughout seasons are simulated for WP1, WP5, WP6 and WP7. WP3 and WP4 appear to be slightly less frequent at the end of the century during JJA and SON seasons, respectively. These slight decreases seem to be more pronounced when considering the RCP8.5 simulations. WP2 and WP8 are the two WP with the most pronounced seasonal changes and are in opposition. Overall, WP2 is slightly less frequent (but its frequency evolution depends on the RCP outputs considered), while WP8 is highly more frequent. These conjoint evolutions are particularly notable for the JJA season. For this season, WP8 frequency is constantly increasing with time for RCP8.5 outputs, while the frequency increase is stopped around the 2060 years for RCP4.5. Oppositely, the WP2 frequency decrease for the same season is stronger when considering RCP8.5 outputs. For the SON season, a strong increase of WP8 is also notable, while a slight decrease of WP4 and WP2 frequencies is found (expect for uncorrected RCP8.5 outputs). For the DJF and MAM seasons, the WP8 appears to be also more frequent, while no particular frequency evolution is found for WP2.
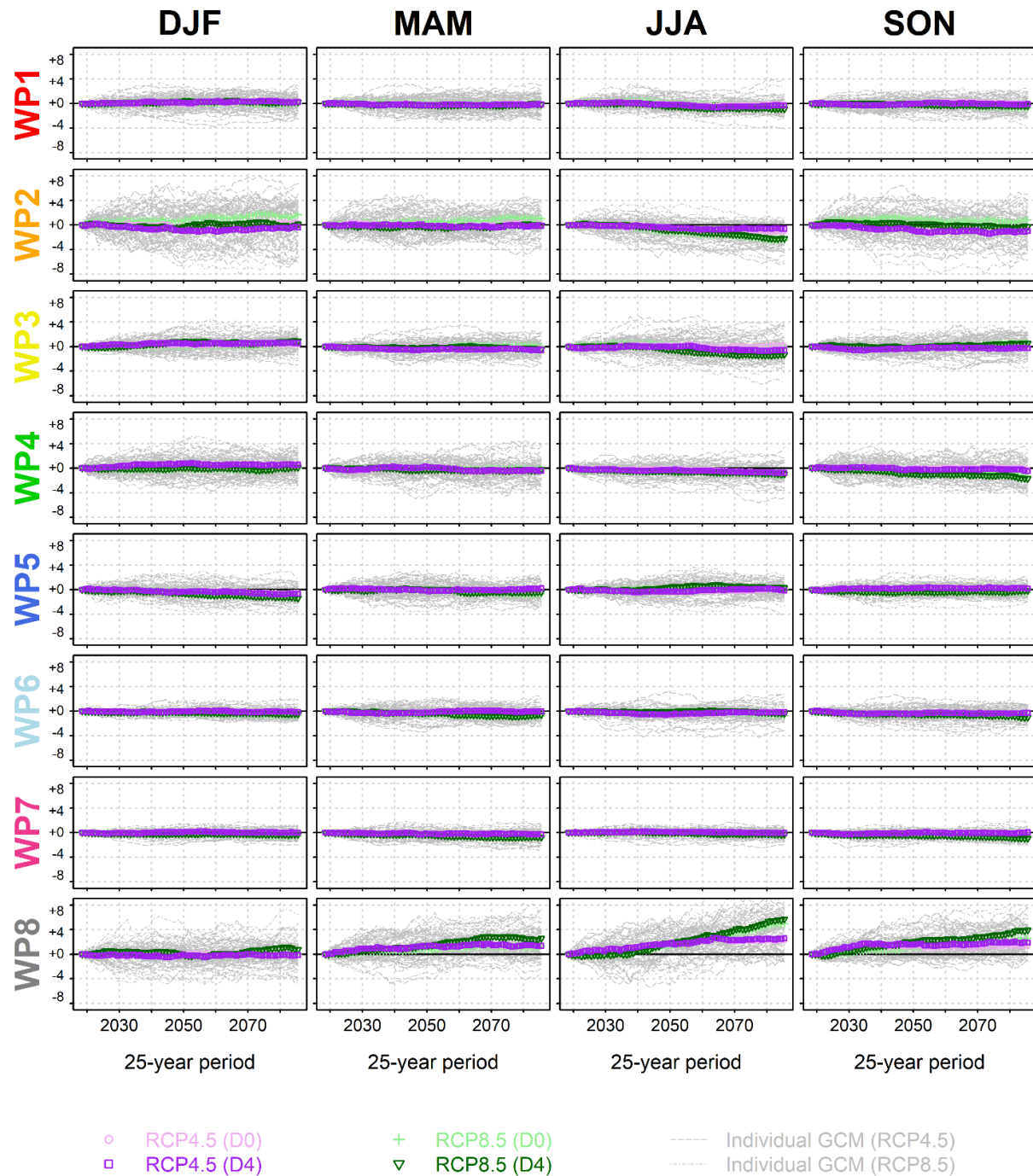
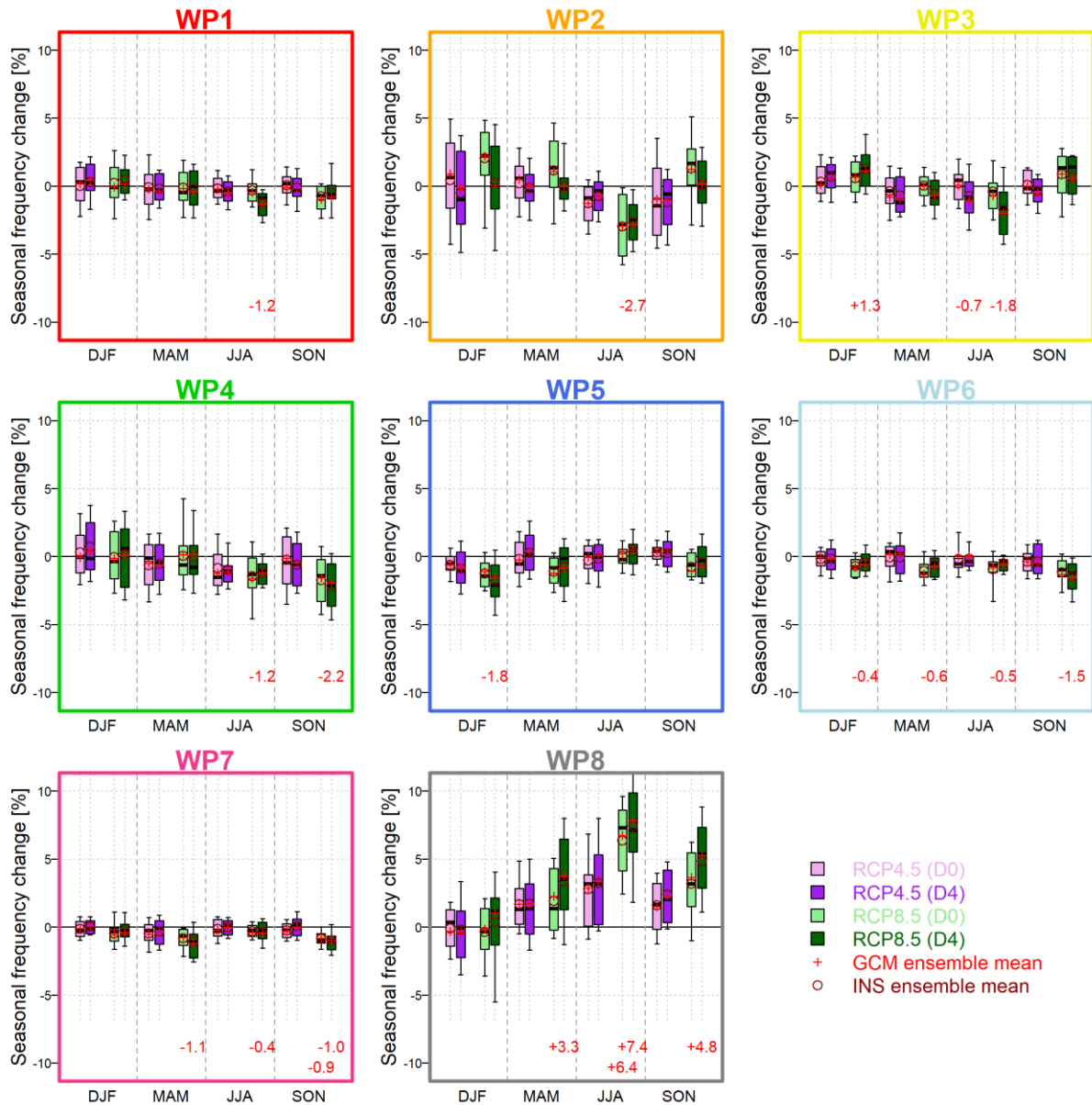**Figure 6:** *Seasonal WP frequency changes (in %) estimated with the GCM ensemble over 68 consecutive 25-year periods, considering RCP4.5 and RCP8.5 simulations, with no bias correction (D0) and with the D4 bias correction method. Changes are relative to the WP frequencies simulated by the GCM ensemble over the first 25-year period (2006-2031). Grey lines are individual GCM WP frequency changes.*

368   Figure 7 summarizes the frequency changes calculated between the 2006-2031 period and the
369   2073-2098 period. A Student's t-Test has been performed for highlighting the significant changes of
370   mean seasonal frequency (p-value < 5%). The dispersion of simulated changes is different depending
371   on the WP, with larger dispersion for WP2, WP4 and WP8 frequencies. WP1 frequency appears to only
372   slightly decrease in JJA months for the RCP8.5 simulations (-1.2%, 95% of the GCM ensemble simulating
373   a decrease), when geopotential height bias are corrected with the D4 method. For WP2, the simulated
374   changes are highly dependent on the season and on the application of a bias correction method. After
375   bias correction, no clear frequency changes are obtained when considering RCP4.5 outputs.
376   Nevertheless, the RCP8.5 outputs show a significant decrease of WP2 frequency for the JJA season
377   with the bias correction method applied (-2.7%, 90% of the GCM ensemble simulating a decrease).
378   WP3 appears to be slightly more frequent for DJF (significant increase of +1.3%, 75% of the GCM
379   ensemble simulating an increase, with D4 correction method), while being less frequent for JJA season
380   (significant decrease of -1.8%, 81% of the GCM ensemble simulating a decrease, with D4 correction
381   method), for the RCP8.5 simulations. The summer decrease of the WP3 frequency is also found in the
382   bias-corrected RCP4.5 simulations (significant decrease of -0.7%, 58% of the GCM ensemble simulating
383   a decrease). WP4 are significantly less frequent in JJA season RCP8.5 (-1.2%, 81% of the GCM ensemble
384   simulating a decrease) scenarios and in SON season for bias corrected RCP8.5 (-2.2%) scenarios. A
385   significant decrease of -1.8% in the DJF season is found for WP5 for the bias corrected RCP8.5
386   simulations (decrease simulated by 81% of the GCM ensemble), while no significant changes are found
387   for the other seasons and outputs. The bias corrected RCP8.5 outputs show significant less WP6 days
388   for the different seasons, with a stronger decrease for the SON season (-1.5%, 95% of the GCM
389   ensemble simulating a decrease).The WP7 is slightly less frequent for MAM, JJA and SON seasons,
390   especially when considering RCP8.5 and bias-corrected outputs (-1.1%, -0.4% and -1.0% for these three
391   seasons, decreases simulated by 81%, 67% and 81% of the GCM ensemble, respectively). Finally, the
392   WP8 frequency is significantly increasing for MAM, JJA and SON seasons. These increases are stronger
393   when considering bias corrected RCP8.5 outputs (+3.3%, +7.4% and +4.8%, increases simulated by
394   81%, 95% and 90% of the GCM ensemble respectively).

395   The summer (JJA) Z_{700} values simulated by the GCM ensemble is increasing with time over the
396   studied domain. The GCM ensemble mean is 3137 m around 2018 and is 3183 m around 2085,
397   considering the RCP8.5 scenario. This increase seems to be correlated with the decrease of the WP2
398   summer frequency and with the increase of the WP8 summer frequency (results not shown).
399   Nevertheless, the WP classification was performed using the Teweles & Wobus (1954) distance (D_{TW}),
400   metric calculated with the geopotential height gradients and not with the absolute values of the
401   geopotential heights. Thus, the temporal increase of the geopotential height absolute values is not
402   influencing the D_{TW} calculation and the simulated increase (decrease) of the seasonal WP8 (WP2)
403   frequency are thus due to changes in general circulation over the studied domain and not due to the
404   global increase of surface pressure in future climate.

405

406

Figure 7: *Seasonal WP frequency changes estimated with the GCM ensemble between 2073-2098*
407
period and 2006-2031 period, considering RCP4.5 and RCP8.5 simulations, with no bias correction (D0)
408
and with the D4 bias correction. The significant changes of mean WP frequency are printed in red color
409
and expressed as percentage of frequency change.
410

5   DISCUSSION AND CONCLUSION

An ensemble of 26 GCM used within the fifth Coupled Model Intercomparison Project (CMIP5) have been analyzed in order firstly to test its ability to reproduce observed seasonal geopotential height climatology over Western Europe, secondly to test its ability to reproduce the seasonal frequencies of eight French WPs previously defined (Garavaglia *et al.*, 2010) and finally to estimate the future seasonal WP frequencies.

Firstly, biases of simulated Z_{1000} and Z_{700} have been quantified over Western Europe for the historical period (here 1979-2004), relatively to the ERAi reanalysis. For Z_{1000}, the GCM ensemble biases have both a strong spatial variability and seasonal variability. For example, the GCM ensemble tends to underestimate the geopotential heights at the highest latitudes of the Western Europe in DJF and MAM seasons, while it tends to overestimate geopotential heights at the same latitudes for the JJA and SON seasons. For Z_{700}, the GCM ensemble tends to overestimate the geopotential heights for the four seasons, with a slighter bias over northern latitudes. These spatial and seasonal variabilities of geopotential biases could advocate the use of spatially and seasonally inhomogeneous bias correction methods on the geopotential height outputs.

Secondly, the ability of the GCM ensemble to reproduce historical WP frequencies has been quantified and revealed that the seasonal variability of the WP frequencies are generally well simulated by the uncorrected GCM ensemble (expect for the WP4), with a slightly worse performance obtained for the DJF season. Nevertheless, the frequencies of the two most frequent WP (WP2 and WP8) are poorly simulated by the ensemble, with WP2 frequencies being strongly overestimated and WP8 strongly underestimated. Similar results have been obtained by Santos *et al.* (2016) by looking at WP frequencies simulated by an ensemble of 22 GCM over Western Europe and showing the overestimation by this other ensemble of the frequency of WP associated with zonal airflow. The use of four different bias correction methods showed that the application of a spatially and temporally nonhomogeneous correction of geopotential height fields (here the correction named D4) improved significantly the simulation of WP frequencies for the four seasons.

Finally, the evolution of the WP frequencies over the next century has been quantified, considering two emission scenarios (RCP4.5 and RCP8.5) and considering one bias correction method (D4) and no bias correction. The WP2, WP4 and WP8 have more pronounced seasonal changes, with WP2 and WP4 being less frequent in JJA and SON seasons, respectively, while WP8 being more frequent over MAM, JJA and SON season. The frequency changes calculated are higher for RCP8.5 simulations than for RCP4.5. Moreover, the temporal evolution of the WP frequencies appears to be constant over time for RCP8.5, while the evolution stops around the year 2060 for the RCP4.5 scenario. The use of a bias correction method is important in this context, since the significant mean changes of WP frequencies are all obtained with bias-corrected outputs (expect the increase of WP8 summer frequency). Nevertheless, the analysis of the temporal evolution of WP frequencies (figure 6) and the distribution of simulated frequency changes (figure 7) showed that the bias-correction method used (D4) is not changing the sign of the mean frequency changes compared to the uncorrected GCM outputs. Note that the use of three other bias correction methods (D1 to D3) leads to the same change signs for the different WP and seasons (results not shown).

452   The strong simulated frequency evolution of WP2 and WP8 is an interesting result, which predicts
453   the climate to be drier with time for France. Thus, WP2 (western oceanic circulation), grouping rainy
454   days over the northern France region, is simulated as less frequent in future summers, while WP8
455   (Anticyclonic situations), which groups non-rainy days over France, is simulated as more frequent in
456   future summers. These evolutions could have significant impacts on French low flows, since Giuntoli
457   *et al.* (2013) recently highlighted strong correlations between these WP frequency and drought
458   severity over France. An increase of the frequency of non-rainy WP is also found in the 22 GCM
459   ensemble studied by Santos *et al.* (2016) when considering RCP8.5 outputs.

460   The bias of CMIP5 GCM in terms of the simulation of the eight French WP frequencies rises several
461   questions, firstly about the WP classification methodology considered here. Thus, Vrac *et al.* (2007)
462   showed that the WP classification method used has an impact on the identified patterns, and also that
463   the choice of a given reanalysis as reference could lead to different WP classifications. Applying
464   different classification methods on the same GCM ensemble and considering other reanalysis as
465   reference would be an interesting perspective, in order to see if similar French WP are identified. In
466   addition, the applied methodology assumes that only the WP frequencies are changing in the future,
467   while WP structures are considered as constant in time. Küttel *et al.* (2010) thus highlighted large
468   changes within type variations for European WP. The application of the methodology developed by
469   Cattiaux *et al.* (2012) could be an interesting perspective in order to fully split the part of changes
470   explained by WP frequencies and the part explained by WP structures, for example.

471   The second question to be raised is the spatial domain considered here for the definition of the WP
472   classification and, consequently, for studying WP frequencies simulated by the GCM ensemble. This
473   domain is rather small (-7.50° to 12.75° of longitude and 37.50° to 50.25° of latitude), thus concerning
474   only a limited grid points for the GCM characterized by a limited atmospheric horizontal resolution. If
475   the WP identified at this spatial scale have relevant characteristics in terms of spatial distribution of
476   surface variables such as precipitation over France, it is possible that the horizontal resolution of GCM
477   are too large for allowing them to identify such regional patterns. Nuissier *et al.* (2011), with a rather
478   similar objective of determining WP leading to heavy precipitation events over southern France, used
479   a larger spatial domain for the WP classification (-24° to +39° of longitude and 25.5° to 63° for latitude).
480   Thus, trying to define French WP over a larger spatial domain is an interesting perspective, in order to
481   quantify the future WP frequencies. The use of Regional Climate Model (RCM) could also be an
482   interesting perspective, even though recent work questioned the ability of RCM to reproduce the daily
483   weather regimes (e.g. Lucas-Picher *et al.*, 2016).

484   Finally, the use of spatially nonhomogeneous bias correction methods for geopotential height fields
485   is questionable, since these corrections change the simulated circulation patterns, transforming the
486   GCM outputs in order to be more similar to the reference ones. Moreover, the biases quantified over
487   the historical period have to be assumed as being stationary over time in order to be applied over the
488   future time period considered, which is a strong hypothesis.

489

490   The ultimate goal of this work was to use simulated future frequencies of particular WPs - known
491   to potentially leading to heavy precipitation events (and then extreme floods) - in order to discuss
492   future precipitation (floods) frequency. Within this framework, only the frequency of future rainfall
493   events is studied, thus splitting frequency (related to circulation dynamic) and intensity (related to
494   thermo-dynamic parameters) of such events. Nevertheless, recent studies highlighted that both

495 frequency and intensity have to be studied for discussing future extreme precipitation (e.g. Hertig *et*
496 *al.,* 2013; Blenkinsop *et al*., 2015) or climate extreme event attribution (e.g. Trenberth *et al.*, 2015).

497   Finally, another interesting future work would be to study the potential shift of WP persistence over
498 the same region and with the same GCM ensemble, since the persistence of rainy or non-rainy WPs is
499 a good indicator for flood or drought frequency and intensity.

500

6   ACKNOWLEDGEMENTS

511

7   BIBLIOGRAPHY

513 Anagnostopoulou C, Tolika K, Maheras P, Kutiel H, Flocas HA. 2008. Performance of the general
514 circulation HadAM3P model in simulating circulation types over the Mediterranean region.
515 *International Journal of Climatology* **28**(2): 185–203. DOI: 10.1002/joc.1521.

516 Belleflamme A, Fettweis X, Erpicum M. 2014. Do global warming-induced circulation pattern changes
517 affect temperature and precipitation over Europe during summer? *International Journal of Climatology*
518 **35**(7): 1484–1499. DOI: 10.1002/joc.4070.

519 Belleflamme A, Fettweis X, Lang C, Erpicum M. 2013. Current and future atmospheric circulation at 500
520 hPa over Greenland simulated by the CMIP3 and CMIP5 global models. *Climate Dynamics* **41**(7–8):
521 2061–2080. DOI: 10.1007/s00382-012-1538-2.

522 Benech B, Brunet H, Jacq V, Payen M, Rivrain J-C, Santurette P. 1993. La catastrophe de Vaison-La-
523 Romaine et les violentes précipitations de septembre 1992: aspects météorologiques. *La Météorologie*
524 (1): 72–90.

525 Blenkinsop S, Chan SC, Kendon EJ, Roberts NM, Fowler HJ. 2015. Temperature influences on intense
526 UK hourly precipitation and dependency on large-scale circulation. *Environmental Research Letters*
527 **10**(5): 054021. DOI: 10.1088/1748-9326/10/5/054021.

528 Boé J, Terray L. 2008. A Weather-Type Approach to Analyzing Winter Precipitation in France:
529 Twentieth-Century Trends and the Role of Anthropogenic Forcing. *Journal of Climate* **21**(13): 3118–
530 3133. DOI: 10.1175/2007JCLI1796.1.

531   Bontron G. 2004. Prévision quantitative des précipitations: adaptation probabiliste par recherche
532   d'analogues. Utilisation des ré-analyses NCEP/NCAR et application aux précipitations du Sud-Est de la
533   France. Institut Polytechnique de Grenoble, PhD thesis, 276 pp.

534   Brigode P, Brissette F, Nicault A, Perreault L, Kuentz A, Mathevet T, Gailhard J. 2016. Streamflow
535   variability over the 1881–2011 period in northern Québec: comparison of hydrological reconstructions
536   based on tree rings and geopotential height field reanalysis. *Climate of the Past* **12**(9): 1785–1804. DOI:
537   10.5194/cp-12-1785-2016.

538   Brigode, P, Bernardara P, Gailhard J, Garavaglia F, Ribstein P, Merz R. 2013a. Optimization of the
539   Geopotential Heights Information Used in a Rainfall-Based Weather Patterns Classification over
540   Austria. International Journal of Climatology 33(6): 1563–1573. DOI:10.1002/joc.3535.

541   Brigode P, Mićović Z, Bernardara P, Paquet E, Garavaglia F, Gailhard J, Ribstein P. 2013b. Linking ENSO
542   and heavy rainfall events over coastal British Columbia through a weather pattern classification.
543   *Hydrology and Earth System Sciences* **17**(4): 1455–1473. DOI: 10.5194/hess-17-1455-2013.

544   Cassano JJ, Uotila P, Lynch A. 2006. Changes in synoptic weather patterns in the polar regions in the
545   twentieth and twenty-first centuries, part 1: Arctic. *International Journal of Climatology* **26**(8): 1027–
546   1049. DOI: 10.1002/joc.1306.

547   Cassou C, Terray L, Hurrell JW, Deser C. 2004. North Atlantic Winter Climate Regimes: Spatial
548   Asymmetry, Stationarity with Time, and Oceanic Forcing. *Journal of Climate* **17**(5): 1055–1068. DOI:
549   10.1175/1520-0442(2004)017<1055:NAWCRS>2.0.CO;2.

550   Cassou C, Terray L, Phillips AS. 2005. Tropical Atlantic Influence on European Heat Waves. *Journal of*
551   *Climate* **18**(15): 2805–2811. DOI: 10.1175/JCLI3506.1.

552   Cattiaux J, Douville H, Ribes A, Chauvin F, Plante C. 2012. Towards a better understanding of changes
553   in wintertime cold extremes over Europe: a pilot study with CNRM and IPSL atmospheric models.
554   *Climate Dynamics* **40**: 2433. DOI: 10.1007/s00382-012-1436-7.

555   Corti S, Molteni F, Palmer TN. 1999. Signature of recent climate change in frequencies of natural
556   atmospheric circulation regimes. *Nature* **398**(6730): 799–802. DOI: 10.1038/19745.

557   Covey C, AchutaRao KM, Cubasch U, Jones P, Lambert SJ, Mann ME, Phillips TJ, Taylor KE. 2003. An
558   overview of results from the Coupled Model Intercomparison Project. *Global and Planetary Change*
559   **37**(1–2): 103–133. DOI: 10.1016/S0921-8181(02)00193-5.

560   Dee DP, Uppala SM, Simmons AJ, Berrisford P, Poli P, Kobayashi S, Andrae U, Balmaseda MA, Balsamo
561   G, Bauer P, Bechtold P, Beljaars ACM, van de Berg L, Bidlot J, Bormann N, Delsol C, Dragani R, Fuentes
562   M, Geer AJ, Haimberger L, Healy SB, Hersbach H, Hólm EV, Isaksen L, Kållberg P, Köhler M, Matricardi
563   M, McNally AP, Monge-Sanz BM, Morcrette J-J, Park B-K, Peubey C, de Rosnay P, Tavolato C, Thépaut
564   J-N, Vitart F. 2011. The ERA-Interim reanalysis: configuration and performance of the data assimilation
565   system. *Quarterly Journal of the Royal Meteorological Society* **137**(656): 553–597. DOI: 10.1002/qj.828.

566   Demuzere M, Werner M, van Lipzig NPM, Roeckner E. 2009. An analysis of present and future ECHAM5
567   pressure fields using a classification of circulation patterns. *International Journal of Climatology* **29**(12):
568   1796–1810. DOI: 10.1002/joc.1821.

569   Dunn-Sigouin E, Son S-W. 2013. Northern Hemisphere blocking frequency and duration in the CMIP5
570   models. *Journal of Geophysical Research* **118**(3): 1179–1188. DOI: 10.1002/jgrd.50143.

571 Garavaglia F, Gailhard J, Paquet E, Lang M, Garçon R, Bernardara P. 2010. Introducing a rainfall
572 compound distribution model based on weather patterns sub-sampling. *Hydrology and Earth System*
573 *Sciences* **14**(6): 951–964. DOI: 10.5194/hess-14-951-2010.

574 Garavaglia F, Lang M, Paquet E, Gailhard J, Garçon R, Renard B. 2011. Reliability and robustness of
575 rainfall compound distribution model based on weather pattern sub-sampling. *Hydrology and Earth*
576 *System Sciences* **15**(2): 519–532. DOI: 10.5194/hess-15-519-2011.

577 Gillett NP, Zwiers FW, Weaver AJ, Stott PA. 2003. Detection of human influence on sea-level pressure.
578 *Nature* **422**(6929): 292–294.

579 Giuntoli I, Renard B, Vidal J-P, Bard A. 2013. Low flows in France and their relationship to large-scale
580 climate indices. *Journal of Hydrology* **482**: 105–118. DOI: 10.1016/j.jhydrol.2012.12.038.

581 Hall   A.   2014.   Projecting   regional   change.   *Science*   **346**(6216):   1461–1462.   DOI:
582 10.1126/science.aaa0629.

583 Handorf D, Dethloff K. 2012. How well do state-of-the-art atmosphere-ocean general circulation
584 models   reproduce   atmospheric   teleconnection   patterns?   *Tellus   A*   **64**(0).   DOI:
585 10.3402/tellusa.v64i0.19777.

586 Haylock MR, Hofstra N, Tank AMG., Klok EJ, Jones PD, New M. 2008. A European daily high-resolution
587 gridded data set of surface temperature and precipitation for 1950–2006. *Journal of Geophysical*
588 *Research* **113**(D20): D20119. DOI: 10.1029/2008JD010201.

589 Hertig E, Jacobeit J. 2014. Variability of weather regimes in the North Atlantic-European area: past and
590 future. *Atmospheric Science Letters* **15**(4): 314–320. DOI: 10.1002/asl2.505.

591 Hertig E, Seubert S, Paxian A, Vogt G, Paeth H, Jacobeit J. 2013. Statistical modelling of extreme
592 precipitation indices for the Mediterranean area under future climate change. *International Journal of*
593 *Climatology* **34**(4): 1132–1156. DOI: 10.1002/joc.3751.

594 Hsu CJ, Zwiers F. 2001. Climate change in recurrent regimes and modes of northern hemisphere
595 atmospheric   variability.   *Journal   of   Geophysical   Research*   **106**(D17):   20145–20159.   DOI:
596 10.1029/2001JD900229.

597 Huth R, Beck C, Philipp A, Demuzere M, Ustrnul Z, Cahynová M, Kyselý J, Tveito OE. 2008. Classifications
598 of Atmospheric Circulation Patterns. *Annals of the New York Academy of Sciences* **1146**(1): 105–152.
599 DOI: 10.1196/annals.1446.019.

600 Küttel M, Luterbacher J, Wanner H. 2010. Multidecadal changes in winter circulation-climate
601 relationship in Europe: frequency variations, within-type modifications, and long-term trends. *Climate*
602 *Dynamics* **36**(5–6): 957–972. DOI: 10.1007/s00382-009-0737-y.

603 Lorenzo MN, Ramos AM, Taboada JJ, Gimeno L. 2011. Changes in Present and Future Circulation Types
604 Frequency in Northwest Iberian Peninsula. *PLoS ONE* **6**(1). DOI: 10.1371/journal.pone.0016201.

605 Lucas-Picher P, Cattiaux J, Bougie A, Laprise R. 2016. How does large-scale nudging in a regional climate
606 model contribute to improving the simulation of weather regimes and seasonal extremes over North
607 America? *Climate Dynamics* **46**(3–4): 929–948. DOI: 10.1007/s00382-015-2623-0.

608   McKendry IG, Stahl K, Moore RD. 2006. Synoptic sea-level pressure patterns generated by a general
609   circulation model: comparison with types derived from NCEP/NCAR re-analysis and implications for
610   downscaling. *International Journal of Climatology* **26**(12): 1727–1736. DOI: 10.1002/joc.1337.

611   Michelangeli P-A, Vautard R, Legras B. 1995. Weather Regimes: Recurrence and Quasi Stationarity.
612   *Journal   of   Atmospheric   Sciences*   **52**:   1237–1256.   DOI: 10.1175/1520-
613   0469(1995)052<1237:WRRAQS>2.0.CO;2.

614   Moss RH, Edmonds JA, Hibbard KA, Manning MR, Rose SK, Vuuren DP van, Carter TR, Emori S, Kainuma
615   M, Kram T, Meehl GA, Mitchell JFB, Nakicenovic N, Riahi K, Smith SJ, Stouffer RJ, Thomson AM, Weyant
616   JP, Wilbanks TJ. 2010. The next generation of scenarios for climate change research and assessment.
617   *Nature* **463**(7282): 747–756. DOI: 10.1038/nature08823.

618   Murawski A, Bürger G, Vorogushyn S, Merz B. 2016. Can local climate variability be explained by
619   weather patterns? A multi-station evaluation for the Rhine basin. *Hydrology and Earth System Sciences*
620   **20**(10): 4283–4306. DOI: 10.5194/hess-20-4283-2016.

621   Nied M, Pardowitz T, Nissen K, Ulbrich U, Hundecha Y, Merz B. 2014. On the relationship between
622   hydro-meteorological patterns and flood types. *Journal of Hydrology* **519**: 3249–3262. DOI:
623   10.1016/j.jhydrol.2014.09.089.

624   Nuissier O, Joly B, Joly A, Ducrocq V, Arbogast P. 2011. A statistical downscaling to identify the large-
625   scale circulation patterns associated with heavy precipitation events over southern France. *Quarterly
626   Journal of the Royal Meteorological Society* **137**(660): 1812–1827. DOI: 10.1002/qj.866.

627   Obled C, Bontron G, Garçon R. 2002. Quantitative precipitation forecasts: a statistical adaptation of
628   model outputs through an analogues sorting approach. *Atmospheric Research* **63**(3–4): 303–324. DOI:
629   10.1016/S0169-8095(02)00038-8.

630   Pastor MA, Casado MJ. 2012. Use of circulation types classifications to evaluate AR4 climate models
631   over the Euro-Atlantic region. *Climate Dynamics* **39**(7–8): 2059–2077. DOI: 10.1007/s00382-012-1449-
632   2.

633   Philipp A, Della-Marta PM, Jacobeit J, Fereday DR, Jones PD, Moberg A, Wanner H. 2007. Long-Term
634   Variability of Daily North Atlantic–European Pressure Patterns since 1850 Classified by Simulated
635   Annealing Clustering. *Journal of Climate* **20**(16): 4065–4095. DOI: 10.1175/JCLI4175.1.

636   Planchon O, Quénol H, Dupont N, Corgne S. 2009. Application of the Hess-Brezowsky classification to
637   the identification of weather patterns causing heavy winter rainfall in Brittany (France). *Natural
638   Hazards and Earth System Sciences* **9**(4): 1161–1173. DOI: 10.5194/nhess-9-1161-2009.

639   Plaut G, Simonnet E. 2001. Large-scale circulation classification, weather regimes, and local climate
640   over France, the Alps and Western Europe. *Climate Research* **17**(3): 303–324. DOI: 10.3354/cr017303.

641   R Core Team. 2016. *R A Language and Environment for Statistical Computing*. R Foundation for
642   Statistical Computing: Vienna, Austria.

643   Renard B, Lall U. 2014. Regional frequency analysis conditioned on large-scale atmospheric or oceanic
644   fields. *Water Resources Research* **50**(12): 9536–9554. DOI: 10.1002/2014WR016277.

645   Sanchez-Gomez E, Somot S, Déqué M. 2009. Ability of an ensemble of regional climate models to
646   reproduce weather regimes over Europe-Atlantic during the period 1961–2000. *Climate Dynamics*
647   **33**(5): 723–736. DOI: 10.1007/s00382-008-0502-7.

648   Santos JA, Belo-Pereira M, Fraga H, Pinto JG. 2016. Understanding climate change projections for
649   precipitation over Western Europe with a weather typing approach. *Journal of Geophysical Research*
650   **121**(3): 2015JD024399. DOI: 10.1002/2015JD024399.

651   Sénési S, Bougeault P, Chèze J-L, Cosentino P, Thepenier R-M. 1996. The Vaison-La-Romaine Flash
652   Flood: Mesoscale Analysis and Predictability Issues. *Weather and Forecasting* **11**(4): 417–442. DOI:
653   10.1175/1520-0434(1996)011<0417:TVLRFF>2.0.CO;2.

654   Sheridan SC, Lee CC. 2010. Synoptic climatology and the general circulation model. *Progress in Physical*
655   *Geography* **34**(1): 101–109. DOI: 10.1177/0309133309357012.

656   Stephenson DB, Hannachi A, O'Neill A. 2004. On the existence of multiple climate regimes. *Quarterly*
657   *Journal of the Royal Meteorological Society* **130**(597): 583–605. DOI: 10.1256/qj.02.146.

658   Taylor KE, Stouffer RJ, Meehl GA. 2012. An overview of CMIP5 and the experiment design. *Bulletin of*
659   *the American Meteorological Society* **93**(4): 485–498. DOI: 10.1175/BAMS-D-11-00094.1.

660   Teweles J, Wobus H. 1954. Verification of prognosis charts. *Bulletin of the American Meteorological*
661   *Society* **35**(10): 455–463.

662   Tramblay Y, Neppel L, Carreau J. 2011. Brief communication - Climatic covariates for the frequency
663   analysis of heavy rainfall in the Mediterranean region. *Natural Hazards and Earth System Sciences*
664   **11**(9): 2463–2468. DOI: 10.5194/nhess-11-2463-2011.

665   Tramblay Y, Neppel L, Carreau J, Najib K. 2013. Non-stationary frequency analysis of heavy rainfall
666   events in southern France. *Hydrological Sciences Journal* **58**(2): 280–294. DOI:
667   10.1080/02626667.2012.754988.

668   Trenberth KE, Fasullo JT, Shepherd TG. 2015. Attribution of climate extreme events. *Nature Climate*
669   *Change* **5**(8): 725–730. DOI: 10.1038/nclimate2657.

670   Ullmann A, Fontaine B, Roucou P. 2014. Euro-Atlantic weather regimes and Mediterranean rainfall
671   patterns: present-day variability and expected changes under CMIP5 projections. *International Journal*
672   *of Climatology* **34**(8): 2634–2650. DOI: 10.1002/joc.3864.

673   Vrac M, Hayhoe K, Stein M. 2007. Identification and intermodel comparison of seasonal circulation
674   patterns over North America. *International Journal of Climatology* **27**(5): 603–620. DOI:
675   10.1002/joc.1422.

676   Wetterhall F, Halldin S, Xu C. 2005. Statistical precipitation downscaling in central Sweden with the
677   analogue method. *Journal of Hydrology* **306**(1–4): 174–190. DOI: 10.1016/j.jhydrol.2004.09.008.

678   Wilby RL, Quinn NW. 2013. Reconstructing multi-decadal variations in fluvial flood risk using
679   atmospheric circulation patterns. *Journal of Hydrology* **487**: 109–121. DOI:
680   10.1016/j.jhydrol.2013.02.038.